Advanced Composites and Hybrid Materials _####################_
https://doi.org/10.1007/s42114-024-00972-w

RESEARCH

Non-exchange bias hysteresis loop shifts in dense composites of soft-hard magnetic nanoparticles: New possibilities for simple reference layers in magnetic devices

Pierfrancesco Maltoni[1,5] · Raúl López-Martín[2] · Elena H. Sánchez[2] · Peter S. Normile[2] · Marianna Vasilakaki[3] · Su Seong Lee[4] · Benito Santos Burgos[2] · Eloy A. López del Castillo[2] · Davide Peddis[5,8] · Chris Binns[2] · Kalliopi Trohidou[3] · Roland Mathieu[1] · Josep Nogués[6,7] · José A. De Toro[2]

Received: 9 January 2024 / Revised: 21 July 2024 / Accepted: 17 September 2024

Abstract

Exchange bias has been extensively studied in both exchange-coupled thin films and nanoparticle composite systems. However, the role of *non*-exchange mechanisms in the overall hysteresis loop bias is far from being understood. Here, dense soft-hard binary nanoparticle composites are used not only as a novel tool to unravel the effect of dipolar interactions on the hysteresis loop shift but also as a new strategy to enhance the bias of any magnet exhibiting an asymmetric magnetization reversal. Mixtures of equally sized, 6.8 nm, soft maghemite (γ-Fe_2O_3) nanoparticles (no bias—symmetric reversal) and hard cobalt doped γ-Fe_2O_3 nanoparticles (large exchange bias—asymmetric reversal) reveal that, for certain fractions of soft particles, the loop shift of the composite can be significantly larger than the exchange-bias field of the hard particles in the mixture. Simple calculations indicate how this emerging phenomenon can be further enhanced by optimizing the parameters of the hard particles (coercivity and loop asymmetry). In addition, the existence of a dipolar-induced loop shift ("dipolar bias") is demonstrated both experimentally and theoretically, where, for example, a bias is induced in the initially unbiased γ-Fe_2O_3 nanoparticles due to the dipolar interaction with the exchange-biased hard nanoparticles. These results open a new paradigm in the large field of hysteresis bias and pave the way for novel approaches to tune loop shifts in magnetic hybrid systems beyond interface exchange coupling.

Keywords Magnetic nanocomposites · Nanoparticles · Magnetic properties · Exchange bias

Pierfrancesco Maltoni and Raúl López-Martín have contributed equally to this work.

✉ Pierfrancesco Maltoni
pierfrancesco.maltoni@edu.unige.it

✉ Raúl López-Martín
raul.lopez@uclm.es

✉ Josep Nogués
josep.nogues@icn2.cat

✉ José A. De Toro
joseangel.toro@uclm.es

[1] Department of Materials Science and Engineering, Uppsala University, Box 35, 751 03 Uppsala, Sweden

[2] Instituto Regional de Investigación Científica Aplicada (IRICA) and Departamento de Física Aplicada, Universidad de Castilla-La Mancha, 13071 Ciudad Real, Spain

[3] Institute of Nanoscience and Nanotechnology, NCSR "Demokritos", 153 10 Agia Paraskevi, Attiki, Greece

[4] Agency for Science, Technology and Research (A*STAR), Institute of Materials Research and Engineering (IMRE), 2 Fusionopolis Way, Innovis #08-03, Singapore 138634, Republic of Singapore

[5] Present Address: Dipartimento Di Chimica E Chimica Industriale, Università Degli Studi Di Genova, Via Dodecaneso 31, 1-16146, Genova, Italy

[6] Catalan Institute of Nanoscience and Nanotechnology (ICN2), CSIC and BIST, Campus UAB, Bellaterra, 08193 Barcelona, Spain

[7] ICREA, Pg. Lluís Companys 23, 08010 Barcelona, Spain

[8] Istituto di Struttura Della Materia, CNR, Nm2-Lab, Monterotondo Scalo, Italy

1 Introduction

Exchange bias usually refers to the shift of the hysteresis loop in the field axis in exchange-coupled ferromagnetic/antiferromagnetic systems. Other related effects, like coercivity enhancement, high order anisotropies, or asymmetric reversal, are typically observed in these systems [1–3]. Such effects have been extensively studied in thin films due to the intriguing fundamental properties and their key role in many spintronic devices [2, 4–11]. Similarly, exchange bias in exchange-coupled core/shell nanoparticles is attracting a great deal of interest [2, 12, 13] due both to its novel basic properties and to the broad range of potential applications (e.g., magnetic recording, permanent magnets, or magnetic hyperthermia, among others) [2, 11–18]. The origin of the exchange bias effect is customarily ascribed to interface exchange-coupling between ferromagnetic and antiferromagnetic counterparts, although it is not limited to this type of systems as this effect has been also reported in ferromagnetic/spin glass systems [19], chemically homogeneous nanoparticles [20], or ferrimagnetic/antiferromagnetic systems [21], among others [2, 22]. However, not all horizontal hysteresis loop shifts are caused by (interfacial) exchange-coupling, and therefore, the term "exchange bias" becomes an inappropriate metonym to refer to different types of loop shifts.

For example, dipolar interactions have recently been shown to play a critical role in certain multilayer systems, namely, in the long-range "exchange bias" in ferromagnetic-antiferromagnetic heterostructures separated by non-magnetic layers [23, 24]. In addition, dipolar-induced exchange-bias-like effects have been described in pseudo-spin valve like structures, i.e., hard and soft ferromagnetic layers separated by a non-magnetic layer [25, 26]. Similar effects have also been observed in hard/soft nanostructured hybrid systems [27]. However, in essence, most of these effects are artifacts due to minor loops effects; namely, the applied field is insufficient to saturate the magnetically hard component of the system. Nevertheless, in dense assemblies of core/shell nanoparticles, it has been suggested both theoretically and experimentally that strong dipolar interactions may indeed lead to the modulation of exchange bias properties [28–32], but only for relatively weak exchange bias fields. In fact, other effects apart from dipolar interactions, like competing anisotropies [33] or Dzyaloshinskii-Moriya interactions (recently reported by Han et al. [34], Lü et al. [35] and Castillo-Sepúlveda et al. [36]), can also lead to loop shifts unrelated to interface exchange coupling.

In this framework, it is appealing to combine particles (whose properties can be individually tuned) into magnetic composites searching for an enhanced overall bias. Besides, such composites are promising to elucidate the nature of diverse effects, particularly those resulting from interparticle dipolar interactions, the topic of recent experimental and theoretical efforts [37–39]. In this context, engineering homogeneous binary dense assemblies of highly uniform nanoparticles offers a simple and controlled scenario to explore different parameters in the resulting loop shifts [40]. Compact nanoparticle systems, created by simply compressing two different types of nanoparticles with distinct properties, offer a straightforward approach to leverage interactions between the constituents for a synergistic enhancement of a specific performance metric in novel hybrid composites [41–43]. In the quest to develop advanced composites, magnetic heterogeneity and interfacial interactions open new possibilities in the search of superior performances in applications such as electromagnetic wave shielding/absorption [44–46]. In the present study, we exploit binary magnetic nanocomposites as a tool to investigate two novel types of bias effects beyond exchange-coupling. Specifically, we investigate composites comprising two different types of iron oxide-based nanoparticles—common ferrimagnetic materials widely used in nanoscience [47–49]—with very different magnetic anisotropy, seeking synergies between their respective hard and soft properties. These nanoparticles not only enable the mentioned synergy, but their well-known synthesis procedure yields monodisperse particles, making the composites ideal systems for studying magnetic properties [40]. Such composites are obtained by a dry compaction process of the nanoparticles previously mixed in the liquid phase, a technique that could easily be scaled up to for industrial purposes [50].

Here, we firstly and most surprisingly demonstrate that if one of the composite constituents exhibits an asymmetric reversal, the overall loop may exhibit an enhanced loop shift and use computational simulations to show how to optimize this effect. Secondly, we establish that a hysteresis bias can be induced in an initially unbiased component purely by dipolar interactions even in properly saturated systems (i.e., excluding minor loop artifacts).

2 Methods

2.1 Experimental details

Two sets of nanoparticles were synthesized using an optimized thermal decomposition route [20, 40]: γ-Fe_2O_3 (maghemite) and cobalt-doped γ-Fe_2O_3 (with a Co:Fe ratio = 1:5), with an average diameter of $d_{TEM} = 6.8 \pm 0.6$ nm; sew Fig. 1a, b. For the synthesis of 6.8 nm γ-Fe_2O_3 nanoparticles, 2.19 g of oleic acid (7.75 mmol, 1.7 eq) and 30 mL

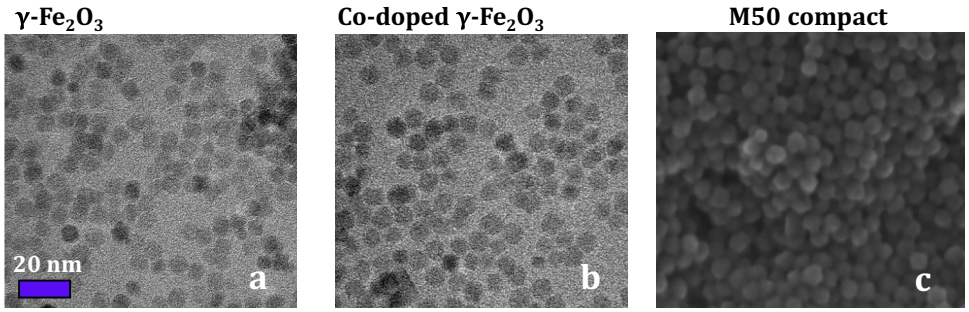

Fig. 1 Electron microscopy images of the hard and soft nanoparticles, and the M50 compact. **a** Transmission electron microscopy (TEM) images of the γ-Fe_2O_3 and **b** Co-doped γ-Fe_2O_3 particles (both 6.8 nm in diameter) used to make all the Mx samples. **c** High-resolution scanning electron microscopy (HR-SEM) image of the M50 compact. The scale bar corresponds to 20 nm, and it is the same for the three panels

of dioctyl ether were added into a two-neck Schlenk flask. After removing water and oxygen under high vacuum, 0.6 mL of $Fe(CO)_5$ (4.56 mmol, 1 eq) was injected into the solution under Ar and heated at 100 °C for 20 min. Subsequently, the solution was further heated to 300 °C at a rate of 4 °C/min under Ar and then refluxed at 300 °C for 90 min. The solution turned black with formation of nanoparticles from decomposition of Fe-oleic acid complexes. The reaction solution was cooled to 60 °C, and 1.02 g of anhydrous $(CH_3)_3NO$ (13.6 mmol) was added to the solution. The resulting mixture was heated at 120 °C for 1 h and then heated to 290 °C at a ramping rate of 4 °C/min. The solution was heated at 290 °C for 1 h and then cooled down to room temperature. Oleic acid-modified nanoparticles were collected by centrifuge through precipitation with addition of acetone. The collected nanoparticles were dispersed in n-hexane and then precipitated again by adding acetone to remove the excess oleic acid.

For the synthesis of the 6.8 nm cobalt-doped γ-Fe_2O_3 nanoparticles, the same procedure used for 6.8 nm γ-Fe_2O_3 nanoparticles was followed, except that 0.5 mL of $Fe(CO)_5$ (3.8 mmol) and 0.13 g of $Co_2(CO)_8$ were added to a two-neck Schlenk flask with oleic acid and octyl ether. During heating, both the metal precursors formed complexes with oleic acid giving a homogeneous solution and decomposed to yield nanoparticles at 300 °C.

The two sets of nanoparticles were mixed in different proportions while still in liquid solution to ensure a homogeneous mixing as already proved elsewhere [40]. The mixed solutions of nanoparticles were washed repeatedly in acetone after centrifugation to remove the coating (oleic acid). A representative compositional EDX mapping of the nanocomposite, confirming the homogeneity, can be found in the Supplementary Section 1. Thermogravimetric analysis shows that an organic residue of only ~ 5%w remains bound to the nanoparticles. The suspension was dried and the resulting powders compacted uniaxially using around 0.8 GPa during 30 s, which is known to yield dense discs with about 60% in packing fraction [51]. The samples are denoted as M*x*, where *x* (=0, 15, 35, 50, 70, 80, 90 or 100%) is the proportion of soft particles.

A Quantum Design MPMS Evercool SQUID magnetometer was employed for the magnetic characterization. Hysteresis loops were obtained at $T = 5$ K after cooling down from room temperature both in zero field and in an applied magnetic field of 50 kOe, which is also the maximum applied field for the hysteresis loops. To confirm the results, additional hysteresis loops for the low *x* samples (with larger saturation field) were performed after cooling down from room temperature in a 90 kOe applied field using a Quantum Design Physical Property Measurement System (PPMS). The same trends are obtained using 90 kOe loops as 50 kOe loops (Supplementary Section 2). Moreover, the hystersis loops with 90 kOe maximum field allow to rule out any "minor loop" effects (Supplementary Fig. 3) [52]. The temperature dependent magnetization curves were recorded after cooling in zero field (ZFC) and in a 5 Oe magnetic field (FC) using the SQUID magnetometer. Note that the *M* axis is normalized to its value at the maximum of the ZFC peak. This normalization approach helps to better understand the differences (ratios) between the ZFC and FC states across different samples, whether they are interacting or non-interacting [53].

The independent magnetic parameters of the soft and hard components in the mixtures were obtained by fitting the experimental loops with a modified Stearn and Cheng model (Eqs. (1) and (2)) [54]. The fitting procedure was optimized by refining step-by-step the parameters, starting with the field and squareness values extracted from the end members (M0 and M100) as initial conditions, and using the calculated M_S and χ from the experimental M*x* loops. As a general approach, three sets of parameters (field-, squareness-, and magnetization-related variables) were refined independently at the beginning, as a means to overcome undesired

effects due to inter-parameter correlation. Particularly, the field-dependent parameters (coercivity and global bias) and the squareness of the soft (symmetric) and hard (asymmetric) loops were found to be strongly correlated, when the soft particle fraction is below 50%, hinting at possible fluctuations due to the observed mathematical effect. To prevent such fluctuations, the squareness parameters ($S_{hard,left}$ and $S_{hard,right}$ for the hard component and S_{soft} for the soft one) were constrained so as not to significantly depart from those of M0 and M100 (Supplementary Section 3).

2.2 Monte carlo simulations

Monte Carlo simulations of the saturated hysteresis loops were carried out using the mesoscopic three-spin model to take into account core/surface morphology, for particles interacting with dipole–dipole interactions [55]. We simulated dense assemblies of spherical nanoparticles with diameter $d=6.8$ nm, and particle concentration $c=60\%$, randomly placed at the nodes of a simple cubic lattice with lattice characteristic lengths Lx, Ly, Lz with $Lx=Ly=Lz=10\alpha$. The parameter α is defined as the smallest inter-particle distance equal to the particle diameter. Each particle is represented by three nearest-neighbor Heisenberg interacting spins (s_1,s_2,s_3), one for the core and two for the surface. The energy of the system in Eq. (1) includes the intra-particle exchange coupling interactions between the three spins at each particle, the core and the surface anisotropy energy terms, the inter-particle dipolar energy term and the Zeeman energy.

$$\begin{aligned} E = &-\tfrac{1}{2}\textstyle\sum_{i=1}^{N}\left[J_{c1}\left(\vec{s}_{1i}\cdot\vec{s}_{2i}\right)+J_{c2}\left(\vec{s}_{1i}\cdot\vec{s}_{3i}\right)+J_{surface}\left(\vec{s}_{2i}\cdot\vec{s}_{3i}\right)\right] \\ &-\textstyle\sum_{i=1}^{N}K_{core}V_1\left(\vec{s}_{1i}\cdot\hat{e}_{1i}\right)^2-\sum_{i=1}^{N}K_{surface}\left[V_2\left(\vec{s}_{2i}\cdot\hat{e}_{2i}\right)^2+V_3\left(\vec{s}_{3i}\cdot\hat{e}_{3i}\right)^2\right] \\ &-\tfrac{1}{2}g\textstyle\sum_{i,j=1,i\neq j}^{N}\left(\sum_{n=1}^{3}m_{ni}\cdot\vec{s}_{ni}\right)D_{ij}\left(\sum_{n=1}^{3}m_{nj}\cdot\vec{s}_{nj}\right) \\ &-\textstyle\sum_{i=1}^{N}\sum_{n=1}^{3}\mu_0 H m_{ni}\left(\vec{s}_{ni}\cdot\hat{e}_h\right) \end{aligned} \tag{1}$$

The parameters used in the simulations were extracted from bulk values of maghemite and $CoFe_2O_4$ as described in reference [40]. Namely, the mesoscopic uniaxial core and surface anisotropy constants for the soft particles were estimated to be $K_{S\_core}=0.17$ and $K_{S\_surface}=15$ and $K_{H\_core}=50$ and $K_{H\_surface}=150$ for the hard particles, with anisotropy axes ($\hat{e}_1$ $\hat{e}_2$ $\hat{e}_3$) randomly oriented. The surface anisotropy is considered to be larger than the core anisotropy due to surface effects, i.e., increased spin canting (ref. [40] for details). The same mesoscopic exchange coupling constants have been used for the hard and soft particles for the core-surface ($j_{c1}=-6.4$, $j_{c2}=3.8$) and surface–surface ($j_{surface}=-0.5$) spin exchange interactions since the corresponding experimental atomic exchange coupling constants of maghemite and Co-ferrite are rather similar [40]. D_{ij} is the dipolar interaction tensor. The dipolar strength is defined as $g=\mu_0(M_sV)^2/4\pi d^3k_BT$ ($T=10$ K) where M_s and V are the experimental values of the saturation magnetization and the volume of each particle and V_1,V_2,V_3 the corresponding volume for each sublattice region found in reference [40]. The dipolar strength g_1 is taken as 13.7 for the pairs of γ-Fe_2O_3 nanoparticles and $g_2=8.4$ for the pairs of Co-doped nanoparticles. For the interaction between maghemite and Co-doped nanoparticles, we set a mean dipolar strength $g_{12}=c_1\cdot g_1+c_2\cdot g_2$ where c_1 and c_2 are the soft nanoparticle and the hard nanoparticle concentrations, respectively (corresponding to $g_{12}=9.2$, 10.3, 11.1, 12.1, 12.6, and 13.2 for $c_1=15\%$, 35%, 50%, 70%, 80%, and 90%, respectively). In the dipolar energy term, we introduce also a weight to each macrospin (m_1 m_2 m_3) to account for the distribution of the volume saturation magnetizations in each region (core, surface) inside the particle. The mesoscopic energy parameters are normalized to the thermal energy k_BT (at temperature $T=10$ K) to be dimensionless. Next, in order to investigate the effect of the strength of the anisotropy of the particles on the observed bias behavior, we have first modified the soft particle core ($K_{S\_core}=0.09$ or 0.35) and surface anisotropy ($K_{S\_surface}=10$ or 30), then the hard particle core ($K_{H\_core}=25$ or 80) and surface anisotropy ($K_{H\_surface}=100$ or 160). Also the effect of the dipolar strength of the soft ($g_1=12.33$ or 15.07) and hard particles ($g_2=7.56$ or 9.24) on the bias behavior have been studied. Note that care was taken to use maximum fields in the simulations sufficient to saturate the hysteresis loops.

3 Results and discussion

Two types of equally sized (6.8 ± 0.6 nm) particles were prepared: γ-Fe_2O_3 nanoparticles (hereon described as "low anisotropy" or "soft") and cobalt doped γ-Fe_2O_3 nanoparticles ("high anisotropy" or "hard"). See Fig. 1a, b and "Methods".

Although at low temperatures the isolated (non-interacting) particles of both systems show a roughly similar saturation magnetization (M_S), they exhibit very different blocking temperature, T_B, and low temperature coercivity, H_C, as can be seen in Supplementary Section 4. In these reference samples, the isolation/dilution of the magnetic particles was efficiently guaranteed by coating with a thick SiO_2 shell (serving as spacer in pressed powders) a fraction of the particles from the corresponding batches [20, 56]. The difference in T_B and H_C between both types of particles indicates that Co doping induces an increase of anisotropy. Crucially for this work, while the γ-Fe_2O_3 nanoparticles exhibit zero loop shift (i.e., no exchange bias), the Co-doped particles show a sizable exchange-bias field, i.e., a horizontal shift, of $H_{EB}=1.20$ kOe at 5 K. Virtually, no difference between the positive and negative M_S (less than 1% of M_S) is found, as further evidence of a properly saturated system [57, 58]. The precise origin of the exchange-bias in the hard particles (an intraparticle effect)

is irrelevant for this study, nonetheless we have included a preliminary discussion in the Supplementary Section 5, where the existence of phase segregation in these particles is ruled out by EELS spectroscopy (see Fig. 8 in that Supplementary Section) and presence of a certain degree of disorder (XRD analysis in Supplementary Section 5) is suggested as the origin of the exchange bias [20, 40, 59–64]. Dense composites made of a single type of particles (with no silica coating) produce a large increase of T_B due to interparticle dipolar interactions (Supplementary Section 4) [53], which, however, barely affect the exchange-bias of the individual particles (from 1.20 in the reference system to 1.28 kOe in the disc made of bare Co-doped particles, see Supplementary Section 4). In fact, this small variation may be driven by subtle changes in the nanoparticle surface upon growing the SiO_2 layer [20].

In the following, to avoid any confusion, we will call "exchange bias," H_{EB}, to the loop shifts that unambiguously stem from interface exchange coupling, an intraparticle effect, whereas the more general term "bias," H_B, will be used for loop shifts caused by a combination of the different mechanisms discussed here. All hysteresis loops were measured at $T = 5$ K after cooling in 50 kOe. All measurements were also conducted using fields beyond the anisotropy field, as reported in the Supplementary Section 2, to exclude the possibility of any minor-loop effects.

As the soft particle content in the mixtures increases several effects take place, the most prominent being a change in the shape of the hysteresis loop, from a simple form in the pure samples (M0 and M100) to a "double loop" shape in the mixed systems (Fig. 2 and Supplementary Section 6). This reflects a relatively weak hard-soft interparticle coupling (given the high anisotropy contrast between them) despite the relatively strong dipolar interactions at play [65, 66], which, as expected, leads to a strong monotonic reduction in the global H_C of the mixtures with increasing x (Fig. 3a). Remarkably, in contrast to H_C, the horizontal shift of the loop has a non-monotonic behavior, exhibiting a maximum at $x = 15\%$ before decreasing for larger contents of soft particles (Fig. 3b). Thus, for moderate amounts of soft particles, the global bias H_B of the composites is surprisingly larger than the exchange bias H_{EB} of the single-phased Co-doped sample (M0), despite the soft particles exhibiting perfectly centered loops (no bias).

In order to safely establish this unexpected enhancement in bias (shaped by just one experimental datapoint in Fig. 3a), and given the weak soft-hard coupling evidenced by the measured double-loops, "superposition loops" were obtained by simply adding the experimental loops of the single-phase samples M100 (soft) and M0 (hard), i.e., as $(softloop)(x) + (hardloop)(1 - x)$, in the whole soft-hard proportion range. The coercivity and bias extracted from these superpositions was added to

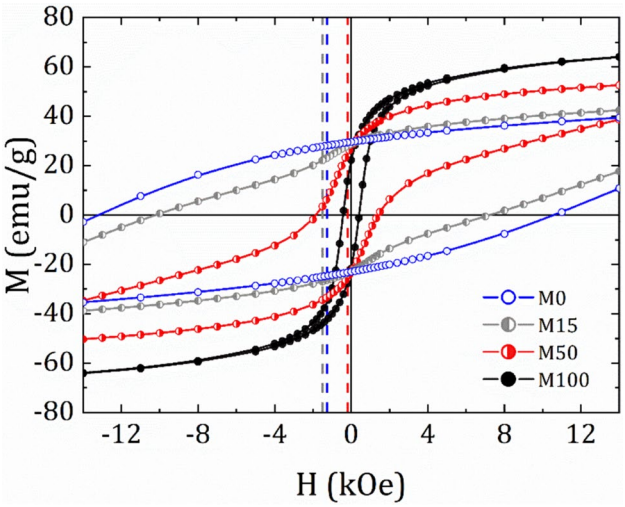

Fig. 2 Hysteresis loops of the M*x* nanocomposites. Low-field region of the hysteresis loops measured at 5 K in selected M*x* systems after field cooling in 50 kOe. The dashed lines near the origin mark the center of the loops (bias field, H_B). See Supplementary Section 6 for the loops of all the samples

Fig. 3a, b (red circles), where it can be seen that the overall trends with x of both H_C and H_B in the experimental and superposition loops are similar, supporting the claim of non-monotonic behavior. In particular, the superposition loops evidence a significant bias enhancement of 25% for $x = 23\%$ (Fig. 3b), demonstrating a 'mathematical' origin for this effect, namely, that the addition of certain differently-shaped loops may give rise to a sizable horizontal shift (H_B). A close inspection of the loop of the hard particles reveals that their magnetization reversal is not completely symmetric, namely the squareness of the descending ($S_{hard,left}$) and ascending ($S_{hard,right}$) branches of the loop are different (see Supplementary Section 7). Asymmetric reversal is usually found in systems with competing anisotropies [67], and in our case, we ascribe it to the spin disorder in the Co-doped nanoparticles (see Supplementary Section 5). To quantify the asymmetry in the reversal of the hard particles, each of the branches of the was fitted to a Stearns and Cheng functions (a relatively simple empirical model [54]).

$$M_{\pm}(H) = \frac{2}{\pi} M_{S,hard} \operatorname{atan}\left[\left(\frac{H + H_{EB,hard} \pm H_{C,hard}}{H_{C,hard}}\right) \tan\left(\frac{\pi S_{hard,\pm}}{2}\right)\right] + \chi H \quad (2)$$

where the $\pm$ symbol indicates the different signs used in the ascending (right) and descending (left) branches of the loops, χ is a high-field susceptibility (see "Methods"), and $H_{EB,hard} \pm H_{C,hard}$ were fixed to the measured values. The resulting squareness parameters of the hard phase are

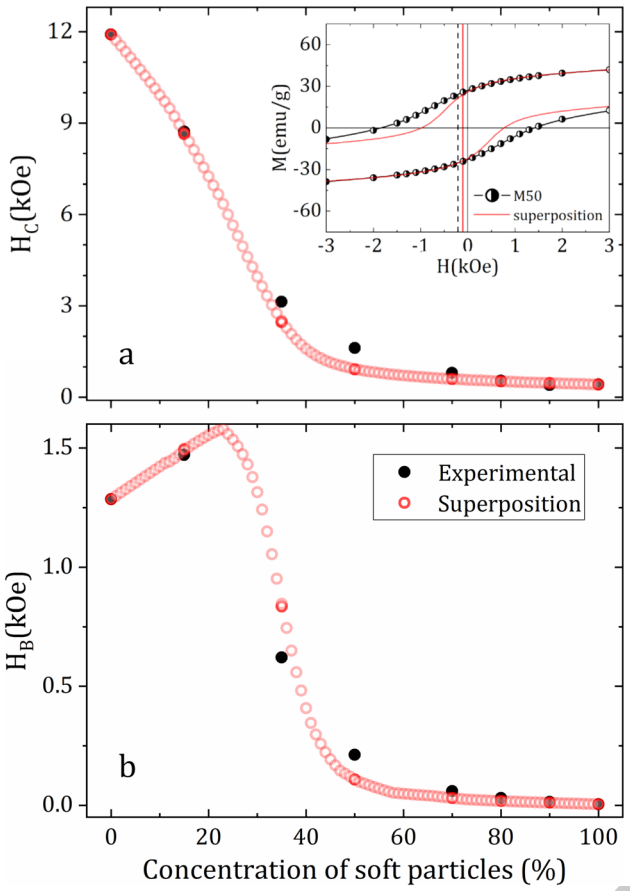

Fig. 3 Bias and coercivity of the binary nanocomposites. Dependence on the concentration of soft particles of **a** the coercivity, H_C, and **b** the bias field, H_B, extracted from the loops measured at 5 K in the dense mixtures (Experimental) and from the weighted superposition of the end members (pure maghemite and Co-doped maghemite) loops (Superposition). The inset in **a** shows the low-field region of the experimental (sample M50) and superposition loops for $x = 50$

$S_{hard,left} = 0.65$, and $S_{hard,right} = 0.56$, i.e., yielding an "asymmetry ratio" $S_{hard,right}/S_{hard,left} = 0.86$). It is this asymmetry in the hard loop which literally shifts the overall loop upon adding a soft component, even when superposing two unbiased loops (see below), as schematized in Fig. 4a.

Once the asymmetric reversal of the hard loop was stablished as the origin of the bias enhancement in Fig. 3b, we investigated the optimization/sensitivity of the effect to the coercivity and asymmetry ratio of the hard component in a given soft-hard mixture. To this purpose, a full array of superposition loops was obtained using the experimental loop for the soft particles (unshifted and symmetric, i.e., with $S_{soft,right} = S_{soft,left} = S_{soft} = 0.32$) and hard loops simulated with different degrees of asymmetric reversal (i.e., different $S_{hard,right}/S_{hard,left}$ ratios, keeping $S_{hard,left}$ fixed at 0.65) and coercivity ($H_{C,hard}$). For clarity and to highlight the role of the reversal asymmetry in the hard component, its exchange-bias was set to zero [$H_{EB,\,hard} = 0$ in Eq. (2)]. For each combination of $S_{hard,right}/S_{hard,left}$ and $H_{C,hard}$, superposition loops were calculated across the whole range of soft particles concentration, x (thus obtaining a "3D array" of loops), and the loop bias H_B was extracted. Shown in the inset of Fig. 4b is an example for the case $x = 28\%$, $S_{hard,right}/S_{hard,left} = 0.86$ and $H_{C,hard} = 12$ kOe (the two latter parameters corresponding to the experimental Co-doped maghemite loop). It can be clearly seen that despite the absence of exchange bias in both these soft and hard loops, their superposition generates a strong shift of $H_B = 860$ Oe. It is then the addition of the hard, asymmetric loop and the symmetric soft loop that produces the loop shift in contrast with the typical interfacial effects.

As can be seen in Fig. 4b, the asymmetry-driven bias of the superposition loops peaks at H_B^{max} at different soft particle proportions (x_{max}) depending on the asymmetry ratio ($S_{hard,right}/S_{hard,left}$) due to the shape of the overall loop. In the same figure, the maximum attained bias obtained for a given asymmetry and the inverse value are different. This fact may seem surprising if one considers how the loops were constructed from the Stearns and Cheng model. However, the simulation considers a fixed squareness for the left branch of the hard loop and sweeps the squareness of the right branch to satisfy the desired asymmetry ratio; thus, the two loops are not related even if their asymmetry ratios are.

The results for H_B^{max} over a large $S_{hard,right}/S_{hard,left}$ and $H_{C,hard}$ range, $H_B^{max}\left(\frac{S_{hard,right}}{S_{hard,left}};H_{C,hard}\right)$, are conveniently plotted as a contour plot in Fig. 4c. The plot, with its white vertical ridge at $S_{hard,right}/S_{hard,left} = 1$, serves to remark that the asymmetry-generated bias appears in all superpositions (see Supplementary Section 8), even if the constituent soft and hard loops are unbiased on their own. Note that loop shifts of several kOe can be obtained for realistically large $S_{hard,right}/S_{hard,left}$ and $H_{C,hard}$ values. As expected, for a given asymmetry ratio, the bias enhancement increases with the hard loop coercivity (see also Supplementary Section 8). It is therefore the combination of both parameters that generates bias upon the introduction of a soft unbiased loop. In short, the results clearly indicate that the enhanced bias observed experimentally in the binary mixtures (Fig. 3b) arises from the shape asymmetry of the magnetization curves of the hard phase ($S_{hard,right}/S_{hard,left} \neq 1$), and not from its horizontal shift. Note that, as probed by the contour plot in Fig. 4c, this effect could be universally exploited in any soft-hard binary system (e.g., even in thin film multilayers) to increase or adjust the overall bias of the ensemble as long as one of the moieties exhibits an asymmetric loop and they are weakly-coupled; i.e., they have a sizable difference in their magnetic anisotropy.

Back to Fig. 3, although the parameters extracted from the experimental and the superposition loops follow similar trends with the soft-hard nanoparticle proportion x, marked

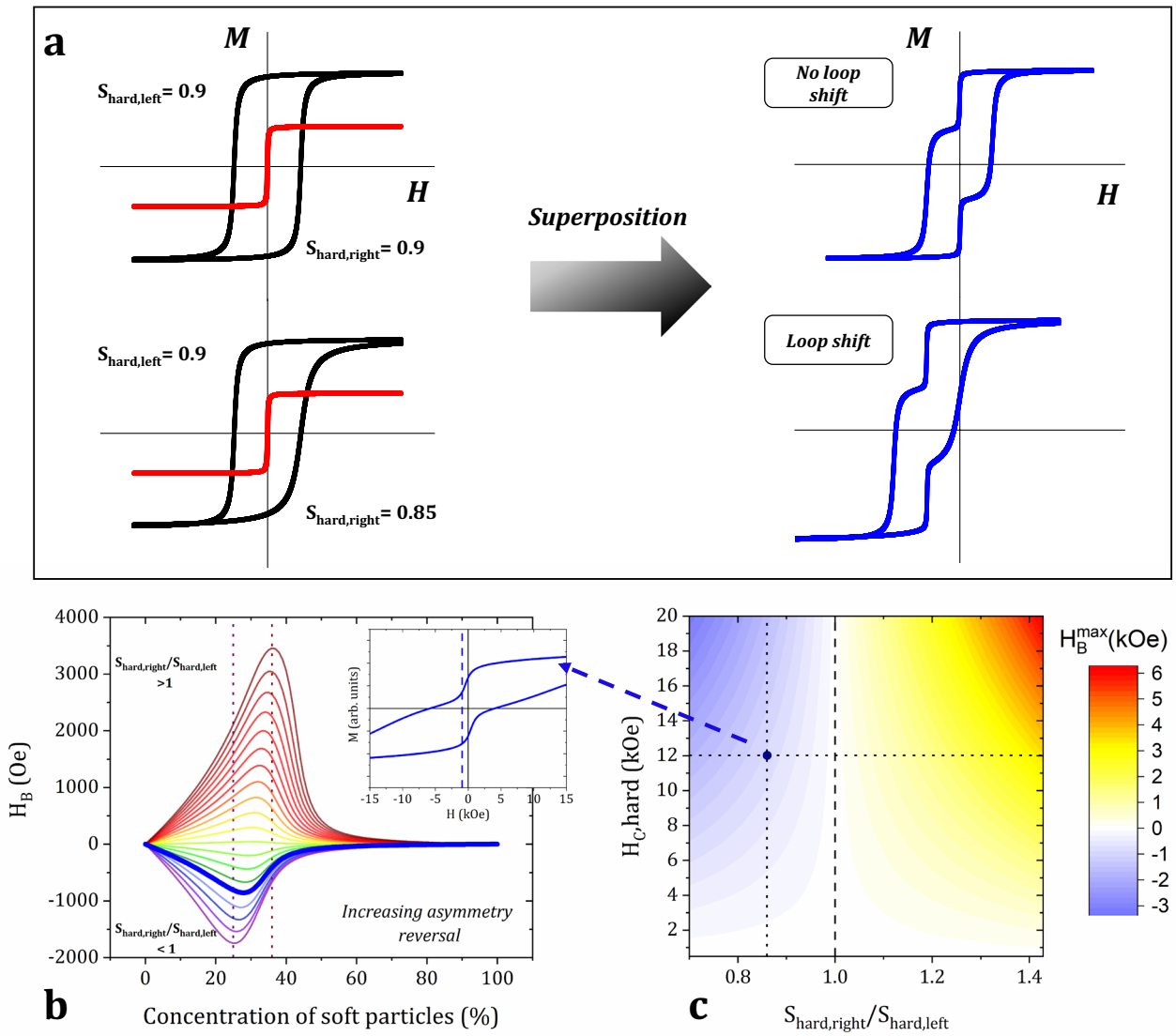

Fig. 4 Numerical investigation of asymmetry-induced bias in binary systems of *un*biased soft and hard particles. **a** Schematic representation of the hard loop asymmetry-driven generation of bias in soft-hard binary nanocomposites. Note that neither the hard nor the soft loops (left hand side) are shifted. The shift of the superposition loop (bottom right) has been exaggerated for clarity. **b** Global bias, H_B, for different hard loop asymmetries [in the range $S_{hard,right}/S_{hard,left} = 0.7$ to 1.43 (=1/0.7)] and $H_{C,hard}$ = "12kOe" as a function of soft content. The thick blue curve corresponds to our experimental series ($S_{hard,right}/S_{hard,left} = 0.86$) after the removal of the hard loop exchange-bias. The inset shows the loop simulated for x_{max}=28% in such series, where the dashed vertical line marks H_B^{max}, the peak value in the blue curve of the main panel. **c** Contour plot exploring the combined influence of the hard loop asymmetry and coercivity on the global H_B^{max} of each concentration series. The position indicated by the blue point (at the intersection of the dotted lines) corresponds to the superposition in the inset of panel **b**. The dashed vertical line corresponds to symmetric loops, $\frac{S_{hard,right}}{S_{hard,left}} = 1$, which yields no bias, $H_B^{max} = 0$. Note that, for clarity, in panels **b** and **c** positive values of H_B correspond to right-shifted loops while negative values correspond to left-shifted loops (in contrast to the convention used in the rest of the article)

differences exist between them for the central samples of the series (see difference plots of Fig. 11 in Supplementary Section 6). Consequently, besides the asymmetry effect described above (an "additive" effect which do not require interparticle interactions), there must be an additional mechanism arising from the dipolar interactions between the particles in our uniform dense mixtures. It is unlikely that the dipolar interactions in our system, quantified by the temperature $T_{dd} = \frac{\mu_0}{4\pi k_B} M_S^2 V\varphi \gg 50K$ (with k_B the Boltzmann constant, M_S the saturation magnetization, V the particle volume, and φ the particle packing fraction) for either soft–soft, hard-hard, and soft-hard combination [53], may affect significantly the strong intraparticle exchange-coupling (and therefore the exchange bias) of the Co-doped particles, the latter having a much larger associated energy [30]. In other words, the ratio T_{ex}/T_{dd} (where

the temperature T_{ex} is proportional to the exchange-coupling energy at the interface; $E_{ex} = H_{EB}V_{FiM}M_S$ [2]) is rather large for small particles such as those studied here. The exchange stiffness constant A_{ex} for the corresponding ferrites ($\sim 10^{-12}$) [68] is two orders of magnitude larger than the dipolar stiffness A_{dip} extracted from a random anisotropy model ($\sim 10^{-14}$) of the present systems [40], confirming that the exchange energies involved are much higher [69, 70]. Indeed, a bibliographic study presented in the SI (Supplementary Section 9) shows that $\frac{T_{ex}}{T_{dd}} \gg\sim 1$ in all the nanocomposites considered except those exhibiting very low exchange bias fields [30, 53, 71, 72].

Thus, it is more likely that the strong dipolar interactions between the two types of particles are mutually influencing the magnetic response of each population and therefore the overall magnetization loop. In this way, the hard particles will "pin" or delay the switching of the softer particles, and vice versa, which in turn determine the coercivity and loop shift of each population. Since the reversal of the hard particles is strongly biased, the pinning effect in the reversal of the soft particles will be correspondingly biased, leading to a dipolar-induced loop shift in the soft particles as illustrated in Figs. 5 and 6. In Fig. 5a, we analyze the largest horizontal separation between the experimental and superposition loops in the low field region (i.e., near the constriction caused by the soft particle reversal). Such distance is larger in the left than in the right branch, which suggests a biased response of the soft particles. Figure 5b plots the difference between the "left" and "right" separations as a function of the soft particle concentration, which decreases upon reducing the content of *hard* particles, thus lending support to the previous statement.

To further test the idea of a dipolar transfer of bias to the soft particles, the experimental hysteresis loops measured in the mixtures were fitted to a double Stearn-Cheng function comprising soft and hard components and allowing individual bias for *both* of them.

$$M_{\pm}(H) = \frac{2}{\pi}M_{S,soft}\text{atan}[(\frac{H + H_{B,soft} \pm H_{C,soft}}{H_{C,soft}})\tan(\frac{\pi S_{soft}}{2})] + \frac{2}{\pi}M_{S,hard}\text{atan}[(\frac{H + H_{B,hard} \pm H_{C,hard}}{H_{C,hard}})\tan(\frac{\pi S_{hard,\pm}}{2})] + \chi H \quad (3)$$

This model factors in the asymmetric reversal of the hard loop, thus decoupling the mathematical effect described above from a possible dipolar-induced bias effect. An example of such a fit is given in Supplementary Section 3. The H_B values obtained for the hard and soft particles ($H_{B,hard}$ and $H_{B,soft}$, respectively) as a function of x confirm the mutual influence between the two particle populations (Fig. 6a). Focusing on the initially unbiased soft particles, the results indicate the appearance of a "dipolar bias" in their magnetization reversal which increases, as expected, with the concentration of hard particles. This trend is analogous to that plotted in Fig. 5b, hence establishing the appearance of "dipolar bias" in the magnetization reversal of the soft nanoparticles in the mixtures. Conversely, the soft particles represent a dragging force favoring the field-alignment of the hard particles moments, which leads to the reduction of both their coercivity (see Supplementary Section 3 and ref.

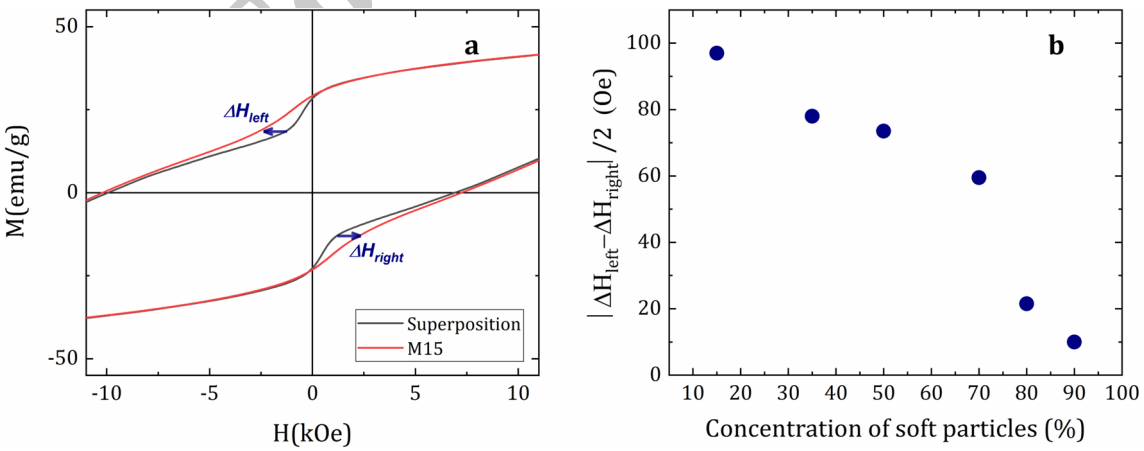

Fig. 5 Analysis of the constriction in the hysteresis loops of the binary nanocomposites. **a** Low-field region of the experimental (M15) and superposition hysteresis loops for $x = 15\%$. The blue arrows indicate the maximum separation in the field axis between the experimental and superposition loops in both the descending (left) and ascending (right) branches, indicating the effect of dipolar interactions in the reversal of the soft particles. **b** Concentration dependence of the difference between those two distances, quantifying the "dipolar bias" transferred to the soft particles

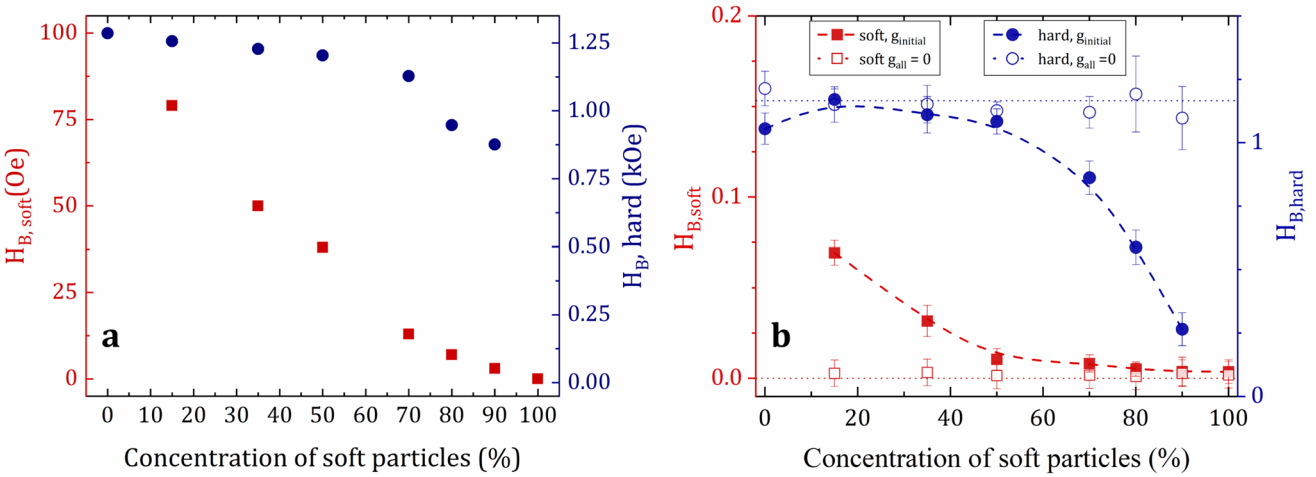

Fig. 6 Bias fields of the individual soft ($H_{B,soft}$) and hard ($H_{B,hard}$) particles extracted from: **a**, fitting the hysteresis loops measured in dense mixtures. **b** the Monte Carlo simulations of such mixtures systems with optimized parameters (filled symbols) and after switching off the dipolar interactions between the particles, i.e., $g_{12}=g_1=g_2=0$ (empty symbols). The loop shift values are dimensionless (see "Methods"). The dotted and dash lines are guides to the eye

[40]) and loop shift for soft particle concentration $x>50\%$ (Fig. 6a).

This finding, which constitutes the foremost demonstration of "dipolar bias" in a nanoparticle system, prompted a Monte Carlo study to further emphasize the role of dipolar interactions, since these simulations allow a straightforward separation of the magnetization reversal of the two populations. The results show precisely the same trends in both the soft and hard particles as those observed experimentally (Fig. 6b, filled symbols). Importantly, the simulations show that the results are similar independently of the chosen parameters, indicative of a robust effect (see Supplementary Section 10). Moreover, in the Monte Carlo simulations, dipolar interactions can be deactivated ad hoc. As can be seen in Fig. 6b (empty symbols), when dipolar interactions between all particles are switched off ($g_1=g_2=g_{12}=0$), the bias of the soft particles remains zero for all concentrations, while H_B for the hard particles remains constant for all x, thus providing further confirmation of dipolar interactions as the origin of the bias induced in the soft particles derived above from the fitting of the experimental loops.

It is important to emphasize that the novel phenomena we describe in the binary mixtures do not depend on the chemical composition, i.e., the choice of nanoparticles, or the origin of the exchange bias (or of the asymmetry) of the hard particles. They are robust mechanisms relying solely on the existence of asymmetry or (in the case of dipolar transfer of bias to the soft particles) exchange bias in the hard nanoparticles, whatever their origin. Additionally, note that while the asymmetry-induced bias is independent of the particle size and magnetization or the packing fraction, the dipolar bias will be strongly influenced by these parameters. Namely, these parameters govern the magnetostatic interactions between the particles, where the dipolar interactions become stronger when the size (and in turn the magnetization) increases. In this sense, a high packing fraction of the nanocomposite (as the one reported here) is vital to have a sizable dipolar bias as well as a highly homogeneous mixing, which maximizes the number of soft-hard neighbors and thus the dipolar transfer of bias.

To conclude, using binary dense nanocomposites has been shown to be instrumental to uncover two new sources of bias (i.e., hysteresis loop shift) different from the usual interface exchange-coupling. Dipolar interactions induce a hysteresis bias (labeled "dipolar bias") in the originally unbiased component (pure soft γ-Fe_2O_3 nanoparticles) due to their coupling with their exchange-biased hard Co-doped γ-Fe_2O_3 neighbors, which act as pinning centers. Importantly, the uniform mixing of nanoparticles in dense composites has been shown to double the effective bias of the ensemble with respect to the simple addition (superposition) of the same components. The second source of bias in soft-hard mixtures, responsible for an unexpected increase in the binary system bias, results from the addition of soft particles (not necessarily interspersed) to hard particles with an asymmetric magnetization reversal. Remarkably, it has been shown that neither interparticle interactions nor individual exchange bias (in the constituent particles) are necessary for the creation of bias in such soft-hard binary nanocomposites; a certain reversal asymmetry in the hard loop is sufficient to induce this novel effect when combined with a soft component. Such asymmetry is typically observed in exchange-coupled nanoparticles, whose bias field may therefore be readily and significantly increased by adding a fraction of soft particles.

4 Conclusions

In summary, our study clearly establishes the existence of two new sources of hysteresis bias in binary soft-hard nanoparticle composites, both of them unrelated to the archetypal exchange bias arising from interface exchange coupling: (i) a "dipolar bias" contribution free from ambiguities due to minor-loop artifacts and (ii) a shift resulting from the addition of soft and asymmetric hard loops, which constitutes a novel strategy to enhance the bias of any hard system with such asymmetric reversal. Thus, non-exchange bias in binary composites sets a new scope in the large field of "exchange bias," i.e., a new tool to understand, optimize, and possibly exploit these "non-exchange bias" effects in the future.

Supplementary Information The online version contains supplementary material available at https://doi.org/10.1007/s42114-024-00972-w.

Acknowledgements This work was supported by the Junta de Castilla-La Mancha (SBPLY/21/180501/000226), UCLM's Plan Propio, and the Swedish Energy Agency (project number 46561-1) and Swedish Research Council (VR) for financial support and providing open access funding. by P.M. also thanks K G Westmans stipendiestiftelse for financially supporting the travel to Universidad de Castilla-La Mancha. J.N. acknowledges the support of grants No. PID2019-106229RB-I00 and PID2022-138588OB-C32 funded by MCIN/AEI/https://doi.org/10.13039/501100011033 and No. 2021-SGR-00651 from the Generalitat de Catalunya. ICN2 is funded by the CERCA programme/Generalitat de Catalunya. The ICN2 is supported by the Severo Ochoa Centres of Excellence programme, Grant CEX2021-001214-S, funded by MCIN/AEI/10.13039.501100011033.

Author contribution The paper and Supplementary Information were written based on the contributions of all authors. J.A.D.T. and J.N. designed the experiment; both coordinated the data analysis and discussion. S.S.L. synthesized the nanoparticles and characterized them by TEM. E.H.S. and P.S.N. prepared the compacts and measured M(H) data. P.M. and R.L.M. are responsible for the magnetic characterization and performed the fittings of the two-phase hysteresis loops. M.V. and K.N.T. performed the Monte Carlo simulations. All authors contributed to the results discussion and revision of the article, which was written mainly by J.A.D.T., J.N., and P.M.

Funding This work was supported by the Spanish Research Agency (AEI, PID2022-142267-I00), the Junta de Castilla-La Mancha (SBPLY/21/180501/000226), UCLM's *Plan Propio*, the Swedish Energy Agency (project number 46561–1), and the Swedish Research Council (VR). P. M. also thanks K G Westmans stipendiestiftelse for financially supporting his stay in Universidad de Castilla-La Mancha. R. L-M. acknowledges his contract to the 'Plan Propio I + D + I' from the UCLM, co-funded by the European Social Fund (2020-PREDUCLM-16730). J. N. acknowledges the support of Grant Nos. PID2019-106229RB-I00 and PID2022-138588OB-C32 funded by MCIN/AEI/https://doi.org/10.13039/501100011033 and Grant No. 2021-SGR-00651 from the Generalitat de Catalunya. ICN2 is funded by the CERCA programme/Generalitat de Catalunya. The ICN2 is supported by the Severo Ochoa Centres of Excellence programme, Grant CEX2021-001214-S, funded by MCIN/AEI/10.13039.501100011033.

Data availability Data sets generated during the current study are available from the corresponding author on reasonable request.

Declarations

Competing interests The authors declare no competing interests.

References

1. Nogués J, Schuller IK (1999) Exchange Bias. J Magn Magn Mater 192(2):203–232. https://doi.org/10.1016/S0304-8853(98)00266-2
2. Nogués J, Sort J, Langlais V, Skumryev V, Suriñach S, Muñoz JS, Baró MD (2005) Exchange bias in nanostructures. Phys Rep 422(3):65–117. https://doi.org/10.1016/j.physrep.2005.08.004
3. Hellman F, Hoffmann A, Tserkovnyak Y, Beach GSD, Fullerton EE, Leighton C, MacDonald AH, Ralph DC, Arena DA, Dürr HA, Fischer P, Grollier J, Heremans JP, Jungwirth T, Kimel AV, Koopmans B, Krivorotov IN, May SJ, Petford-Long AK, Rondinelli JM, Samarth N, Schuller IK, Slavin AN, Stiles MD, Tchernyshyov O, Thiaville A, Zink BL (2017) Interface-induced phenomena in magnetism. Rev Mod Phys 89(2):025006. https://doi.org/10.1103/RevModPhys.89.025006
4. Jensen CJ, Quintana A, Quarterman P, Grutter AJ, Balakrishnan PP, Zhang H, Davydov AV, Zhang X, Liu K (2023) Nitrogen-based magneto-ionic manipulation of exchange bias in CoFe/MnN heterostructures. ACS Nano 17(7):6745–6753. https://doi.org/10.1021/acsnano.2c12702
5. Qin P, Yan H, Wang X, Chen H, Meng Z, Dong J, Zhu M, Cai J, Feng Z, Zhou X, Liu L, Zhang T, Zeng Z, Zhang J, Jiang C, Liu Z (2023) Room-temperature magnetoresistance in an all-antiferromagnetic tunnel junction. Nature 613(7944):485–489. https://doi.org/10.1038/s41586-022-05461-y
6. Lin P-H, Yang B-Y, Tsai M-H, Chen P-C, Huang K-F, Lin H-H, Lai C-H (2019) Manipulating exchange bias by spin–orbit torque. Nat Mater 18(4):335–341. https://doi.org/10.1038/s41563-019-0289-4
7. Ma S, Li G, Li Z, Zhang Y, Lu H, Gao Z, Wu J, Long G, Huang Y (2022) 2D magnetic semiconductor Fe_3GeTe_2 with few and single layers with a greatly enhanced intrinsic exchange bias by liquid-phase exfoliation. ACS Nano 16(11):19439–19450. https://doi.org/10.1021/acsnano.2c09143
8. Wu X, Wang H, Liu H, Wang Y, Chen X, Chen P, Li P, Han X, Miao J, Yu H, Wan C, Zhao J, Chen S (2022) Antiferromagnetic–ferromagnetic heterostructure-based field-free terahertz emitters. Adv Mater 34(42):2204373. https://doi.org/10.1002/adma.202204373
9. Yan S, Choi D-J, Burgess JAJ, Rolf-Pissarczyk S, Loth S (2015) Control of quantum magnets by atomic exchange bias. Nat Nanotechnol 10(1):40–45. https://doi.org/10.1038/nnano.2014.281
10. Lee S, Kang J, Kim J, Kim N, Han D, Lee T, Ko S, Yang J, Lee S, Lee S, Koh D, Kang M, Lee J, Noh S, Lee H, Kwon J, Baek SC, Kim K, Park B (2022) Spintronic physical unclonable functions based on field-free spin–orbit-torque switching. Adv Mater 34(45):2203558. https://doi.org/10.1002/adma.202203558
11. Yang Q, Mishra R, Cen Y, Shi G, Sharma R, Fong X, Yang H (2022) Spintronic integrate-fire-reset neuron with stochasticity for neuromorphic computing. Nano Lett 22(21):8437–8444. https://doi.org/10.1021/acs.nanolett.2c02409
12. López-Ortega A, Estrader M, Salazar-Alvarez G, Roca AG, Nogués J (2015) Applications of exchange coupled bi-magnetic hard/soft and soft/hard magnetic core/shell nanoparticles. Phys Rep 553:1–32. https://doi.org/10.1016/j.physrep.2014.09.007
13. Omelyanchik A, Villa S, Vasilakaki M, Singh G, Ferretti AM, Ponti A, Canepa F, Margaris G, Trohidou KN, Peddis D (2021) Interplay between inter- and intraparticle interactions in

bi-magnetic core/shell nanoparticles. Nanoscale Adv 3(24):6912–6924. https://doi.org/10.1039/D1NA00312G
14. Zákutná D, Rouzbeh N, Nižňanský D, Duchoň J, Qdemat A, Kentzinger E, Honecker D, Disch S (2023) Magnetic coupling in cobalt-doped iron oxide core–shell nanoparticles: exchange pinning through epitaxial alignment. Chem Mater 35(6):2302–2311. https://doi.org/10.1021/acs.chemmater.2c02813
15. Lottini E, López-Ortega A, Bertoni G, Turner S, Meledina M, Van Tendeloo G, de Julián Fernández C, Sangregorio C (2016) Strongly exchange coupled corelshell nanoparticles with high magnetic anisotropy: a strategy toward rare-earth-free permanent magnets. Chem Mater 28(12):4214–4222. https://doi.org/10.1021/acs.chemmater.6b00623
16. De Toro JA, Marques DP, Muñiz P, Skumryev V, Sort J, Givord D, Nogués J (2015) High temperature magnetic stabilization of cobalt nanoparticles by an antiferromagnetic proximity effect. Phys Rev Lett 115(5):057201. https://doi.org/10.1103/PhysRevLett.115.057201
17. Narayanaswamy V, Jagal J, Khurshid H, Al-Omari IA, Haider M, Kamzin AS, Obaidat IM, Issa B (2022) Hyperthermia of magnetically soft-soft core-shell ferrite nanoparticles. Int J Mol Sci 23(23):14825. https://doi.org/10.3390/ijms232314825
18. Vasilakaki M, Trohidou KN, Nogués J (2015) Enhanced magnetic properties in antiferromagnetic-core/ferrimagnetic-shell nanoparticles. Sci Rep 5(1):9609. https://doi.org/10.1038/srep09609
19. Ali M, Adie P, Marrows CH, Greig D, Hickey BJ, Stamps RL (2007) Exchange Bias using a spin glass. Nat Mater 6(1):70–75. https://doi.org/10.1038/nmat1809
20. De Toro JA, Vasilakaki M, Lee SS, Andersson MS, Normile PS, Yaacoub N, Murray P, Sánchez EH, Muñiz P, Peddis D, Mathieu R, Liu K, Geshev J, Trohidou KN, Nogués J (2017) Remanence plots as a probe of spin disorder in magnetic nanoparticles. Chem Mater 29(19):8258–8268. https://doi.org/10.1021/acs.chemmater.7b02522
21. Estrader M, López-Ortega A, Estradé S, Golosovsky IV, Salazar-Alvarez G, Vasilakaki M, Trohidou KN, Varela M, Stanley DC, Sinko M, Pechan MJ, Keavney DJ, Peiró F, Suriñach S, Baró MD, Nogués J (2013) Robust antiferromagnetic coupling in hard-soft bi-magnetic core/shell nanoparticles. Nat Commun 4(1):2960. https://doi.org/10.1038/ncomms3960
22. Nordblad P (2015) Tuning exchange bias. Nat Mater 14(7):655–656. https://doi.org/10.1038/nmat4331
23. Torres F, Morales R, Schuller IK, Kiwi M (2017) Dipole-induced exchange bias. Nanoscale 9(43):17074–17079. https://doi.org/10.1039/C7NR05491B
24. Bollero A, Neu V, Baltz V, Serantes D, Cuñado JLF, Pedrosa J, Palmero EM, Seifert M, Dieny B, del Real RP, Vázquez M, Chubykalo-Fesenko O, Camarero J (2020) An extraordinary chiral exchange-bias phenomenon: engineering the sign of the bias field in orthogonal bilayers by a magnetically switchable response mechanism. Nanoscale 12(2):1155–1163. https://doi.org/10.1039/C9NR08852K
25. Zha CL, Nogués J, Åkerman J (2009) Exchange bias in L10 (111)-oriented fept-based pseudo spin valves. IEEE Trans Magn 45(10):3881–3884. https://doi.org/10.1109/TMAG.2009.2024122
26. Hierro-Rodriguez A, Teixeira JM, Rodriguez-Rodriguez G, Rubio H, Vélez M, Álvarez-Prado LM, Martín JI, Alameda JM (2015) Unravelling the tunable exchange bias-like effect in magnetostatically-coupled two dimensional hybrid (hard/soft) composites. Nanotechnology 26(22):225302. https://doi.org/10.1088/0957-4484/26/22/225302
27. González JM, Montero MI, Raposo V, Hernando A (2000) On the relationship between the hysteresis loop shift and the dipolar interactions in hard–soft nanocomposite samples. J Magn Magn Mater 221(1–2):187–195. https://doi.org/10.1016/S0304-8853(00)00526-6
28. da Silva FG, Vasilakaki M, Gomes RC, Aquino R, Campos AFC, Dubois E, Perzynski R, Depeyrot J, Trohidou K (2022) A numerical study on the interplay between the intra-particle and interparticle characteristics in bimagnetic soft/soft and hard/soft ultrasmall nanoparticle assemblies. Nanoscale Adv 4(18):3777–3785. https://doi.org/10.1039/d1na00894c
29. Dolci M, Liu Y, Liu X, Leuvrey C, Derory A, Begin D, Begin-Colin S, Pichon BP (2018) Exploring exchange bias coupling in $Fe_{3-\delta}O_4$ @CoO core-shell nanoparticle 2D assemblies. Adv Funct Mater 28(26):1706957. https://doi.org/10.1002/adfm.201706957
30. Liu Y, Liu X, Dolci M, Leuvrey C, Pardieu E, Derory A, Begin D, Begin-Colin S, Pichon BP (2018) Investigation of the collective properties in monolayers of exchange-biased $Fe_{3-\delta}O_4$@CoO core-shell nanoparticles. J Phys Chem C 122(30):17456–17464. https://doi.org/10.1021/acs.jpcc.8b04615
31. Cabreira-Gomes R, G Silva F, Aquino R, Bonville P, Tourinho FA, Perzynski R, Depeyrot J (2014) Exchange bias of $MnFe_2O_4$ at γ-Fe_2O_3 and $CoFe_2O_4$ at γ-Fe_2O_3 core/shell nanoparticles. J Magn Magn Mater 368:409–414. https://doi.org/10.1016/j.jmmm.2014.03.003
32. Silva FG, Aquino R, Tourinho FA, Stepanov VI, Raikher YL, Perzynski R, Depeyrot J (2013) The role of magnetic interactions in exchange bias properties of $MnFe_2O_4$ @ γ -Fe_2O_3 core/shell nanoparticles. J Phys D Appl Phys 46(28):285003. https://doi.org/10.1088/0022-3727/46/28/285003
33. Bollero A, Dieny B, Sort J, Buchanan KS, Landis S, Nogués J (2008) Enhanced exchange bias effects in a nanopatterned system consisting of two perpendicularly coupled ferromagnets. Appl Phys Lett 92(2):022508. https://doi.org/10.1063/1.2833124
34. Han D-S, Kim N-H, Kim J-S, Yin Y, Koo J-W, Cho J, Lee S, Kläui M, Swagten HJM, Koopmans B, You C-Y (2016) Asymmetric hysteresis for probing Dzyaloshinskii-Moriya interaction. Nano Lett 16(7):4438–4446. https://doi.org/10.1021/acs.nanolett.6b01593
35. Lü WM, Saha S, Wang XR, Liu ZQ, Gopinadhan K, Annadi A, Zeng SW, Huang Z, Bao BC, Cong CX, Venkatesan M, Yu T, Coey JMD, Ariando, Venkatesan T (2016) Long-range magnetic coupling across a polar insulating layer. Nat Commun 7(1):11015. https://doi.org/10.1038/ncomms11015
36. Castillo-Sepúlveda S, Corona RM, Kiwi M, Carvalho-Santos VL, Altbir D (2024) Dzyaloshinskii-Moriya bias in a free-standing asymmetric homogeneous nanodisk. Results Phys 56:107246. https://doi.org/10.1016/j.rinp.2023.107246
37. Das D, Alam A (2021) Conical Order, Magnetic compensation, and sign reversible exchange bias in spinel structured AB_2O_4 compounds: a Monte Carlo study. Phys Rev Mater 5(4):044404. https://doi.org/10.1103/PhysRevMaterials.5.044404
38. Goswami S, Gupta P, Nayak S, Bedanta S, Iglesias Ò, Chakraborty M, De D (2022) Dependence of exchange bias on interparticle interactions in Co/CoO core/shell nanostructures. Nanomaterials 12(18):3159. https://doi.org/10.3390/nano12183159
39. Martínez-García JC, Rivas M, García JA (2015) Induced ferro-ferromagnetic exchange bias in nanocrystalline systems. J Magn Magn Mater 377:424–429. https://doi.org/10.1016/j.jmmm.2014.10.123
40. Sánchez EH, Vasilakaki M, Lee SS, Normile PS, Muscas G, Murgia M, Andersson MS, Singh G, Mathieu R, Nordblad P, Ricci PC, Peddis D, Trohidou KN, Nogués J, De Toro JA (2020) Simultaneous individual and dipolar collective properties in binary assemblies of magnetic nanoparticles. Chem Mater 32(3):969–981. https://doi.org/10.1021/acs.chemmater.9b03268
41. Guo J, Chen Z, Abdul W, Kong J, Khan MA, Young DP, Zhu J, Guo Z (2021) Tunable positive magnetoresistance of magnetic polyaniline nanocomposites. Adv Compos Hybrid Mater 4(3):534–542. https://doi.org/10.1007/s42114-021-00242-z

42. Ma R, Cui B, Hu D, El-Bahy SM, Wang Y, Azab IHEl, Elnaggar AY, Gu H, Mersal GAM, Huang M, Murugadoss V (2022) Enhanced energy storage of lead-free mixed oxide core double-shell barium strontium zirconate titanate@magnesium aluminate@zinc oxide-boron trioxide-silica ceramic nanocomposites. Adv Compos Hybrid Mater 5(2):1477–1489. https://doi.org/10.1007/s42114-022-00509-z
43. Ovejero JG, Spizzo F, Morales MP, Del Bianco L (2021) Mixing iron oxide nanoparticles with different shape and size for tunable magneto-heating performance. Nanoscale 13(11):5714–5729. https://doi.org/10.1039/D0NR09121A
44. Li F, Bi Z, Kimura H, Li H, Liu L, Xie X, Zhang X, Wang J, Sun X, Ma Z, Du W, Hou C (2023) Energy- and cost-efficient salt-assisted synthesis of nitrogen-doped porous carbon matrix decorated with nickel nanoparticles for superior electromagnetic wave absorption. Adv Compos Hybrid Mater 6(4):133. https://doi.org/10.1007/s42114-023-00710-8
45. Li F, Wu N, Kimura H, Wang Y, Xu BB, Wang D, Li Y, Algadi H, Guo Z, Du W, Hou C (2023) Initiating binary metal oxides microcubes electromagnetic wave absorber toward ultrabroad absorption bandwidth through interfacial and defects modulation. Nano-Micro Lett 15(1):220. https://doi.org/10.1007/s40820-023-01197-0
46. Cai B, Zhou L, Zhao P-Y, Peng H-L, Hou Z-L, Hu P, Liu L-M, Wang G-S (2024) Interface-Induced dual-pinning mechanism enhances low-frequency electromagnetic wave loss. Nat Commun 15(1):3299. https://doi.org/10.1038/s41467-024-47537-5
47. Khan I, Morishita S, Higashinaka R, Matsuda TD, Aoki Y, Kuzmann E, Homonnay Z, Katalin S, Pavić L, Kubuki S (2021) Synthesis, characterization and magnetic properties of ε-Fe_2O_3 nanoparticles prepared by sol-gel method. J Magn Magn Mater 538:168264. https://doi.org/10.1016/j.jmmm.2021.168264
48. Wang T, Fan Z, Xue W, Yang H, Li R-W, Xu X (2023) Controlled growth and size-dependent magnetic domain states of 2D γ-Fe_2O_3. Nano Lett 23(22):10498–10504. https://doi.org/10.1021/acs.nanolett.3c03276
49. Zhang X, Wang Q, Tang Y, Fan G, Hao C, Liu Y (2024) Decoration of conjugated polyacene quinone radical (PAQR) with Fe_3O_4 nanospheres achieving improved impedance matching and electromagnetic wave absorption. Mater Today Phys 41:101349. https://doi.org/10.1016/j.mtphys.2024.101349
50. Tan DHS, Meng YS, Jang J (2022) Scaling up high-energy-density sulfidic solid-state batteries: a lab-to-pilot perspective. Joule 6(8):1755–1769. https://doi.org/10.1016/j.joule.2022.07.002
51. Normile PS, Andersson MS, Mathieu R, Lee SS, Singh G, De Toro JA (2016) Demagnetization effects in dense nanoparticle assemblies. Appl Phys Lett 109(15):152404. https://doi.org/10.1063/1.4964517
52 Harres A, Mikhov M, Skumryev V, Andrade AMHde, Schmidt JE, Geshev J (2016) Criteria for saturated magnetization loop. J Magn Magn Mater 402:76–82. https://doi.org/10.1016/j.jmmm.2015.11.046
53. Sánchez EH, Vasilakaki M, Lee SS, Normile PS, Andersson MS, Mathieu R, López-Ortega A, Pichon BP, Peddis D, Binns C, Nordblad P, Trohidou K, Nogués J, De Toro JA (2022) Crossover from individual to collective magnetism in dense nanoparticle systems: local anisotropy versus dipolar interactions. Small 18:2106762 https://doi.org/10.1002/smll.202106762
54. Stearns MB, Cheng Y (1994) Determination of para- and ferromagnetic components of magnetization and magnetoresistance of granular Co/Ag films (invited). J Appl Phys 75(10):6894–6899. https://doi.org/10.1063/1.356773
55. Margaris G, Trohidou KN, Nogués J (2012) Mesoscopic model for the simulation of large arrays of bi-magnetic core/shell nanoparticles. Adv Mater 24(31):4331–4336. https://doi.org/10.1002/adma.201200615
56. Andersson MS, Mathieu R, Lee SS, Normile PS, Singh G, Nordblad P, De TJA (2015) Size-dependent surface effects in maghemite nanoparticles and its impact on interparticle interactions in dense assemblies. Nanotechnology 26(47):475703. https://doi.org/10.1088/0957-4484/26/47/475703
57. Salazar-Alvarez G, Sort J, Suriñach S, Baró MD, Nogués J (2007) Synthesis and size-dependent exchange bias in inverted core-shell MnO|Mn_3O_4 nanoparticles. J Am Chem Soc 129(29):9102–9108. https://doi.org/10.1021/ja0714282
58. Nogués J, Leighton C, Schuller IK (2000) Correlation between antiferromagnetic interface coupling and positive exchange bias. Phys Rev B 61(2):1315–1317. https://doi.org/10.1103/PhysRevB.61.1315
59. Vasilakaki M, Trohidou KN (2009) Numerical study of the exchange-bias effect in nanoparticles with ferromagnetic core/ferrimagnetic disordered shell morphology. Phys Rev B - Condens Matter Mater Phys 79(14):144402. https://doi.org/10.1103/PhysRevB.79.144402
60. Topkaya R, Akman Ö, Kazan S, Aktaş B, Durmus Z, Baykal A (2012) Surface spin disorder and spin-glass-like behaviour in manganese-substituted cobalt ferrite nanoparticles. J Nanoparticle Res 14(10):1156. https://doi.org/10.1007/s11051-012-1156-2
61. Kodama RH, Berkowitz AE, Mc Niff EJ, Foner S (1996) Surface spin disorder in $NiFe_2O_4$ nanoparticles. Phys Rev Lett 77(2):394–397. https://doi.org/10.1103/PhysRevLett.77.394
62. Muzzi B, Albino M, Petrecca M, Innocenti C, de Julián Fernández C, Bertoni G, Ibarra MR, Christensen M, Avdeev M, Marquina C, Sangregorio C (2023) Defect-engineering by solvent mediated mild oxidation as a tool to induce exchange bias in metal doped ferrites. Small Methods 7(11):2300647 https://doi.org/10.1002/smtd.202300647
63. Martínez B, Obradors X, Balcells L, Rouanet A, Monty C (1998) Low temperature surface spin-glass transition in γ-Fe_2O_3 nanoparticles. Phys Rev Lett 80(1):181–184. https://doi.org/10.1103/PhysRevLett.80.181
64. Zavaliche F, Bensebaa F, L'Ecuyer P, Veres T, Cochrane RW (2005) The role of non-collinear spins on the magnetic properties of uncoupled nanometer-size particles. J Magn Magn Mater 285(1):204–209. https://doi.org/10.1016/j.jmmm.2004.07.042
65. Chen J, Ye X, Oh SJ, Kikkawa JM, Kagan CR, Murray CB (2013) Bistable magnetoresistance switching in exchange-coupled $CoFe_2O_4$-Fe_3O_4 binary nanocrystal superlattices by self-assembly and thermal annealing. ACS Nano 7(2):1478–1486. https://doi.org/10.1021/nn3052617
66. Zeng H, Li J, Liu JP, Wang ZL, Sun S (2002) Exchange-coupled nanocomposite magnets by nanoparticle self-assembly. Nature 420(November):395–398. https://doi.org/10.1038/nature01233.1
67. Camarero J, Sort J, Hoffmann A, García-Martín JM, Dieny B, Miranda R, Nogués J (2005) Origin of the asymmetric magnetization reversal behavior in exchange-biased systems: competing anisotropies. Phys Rev Lett 95(5):057204. https://doi.org/10.1103/PhysRevLett.95.057204
68. Coey JMD (2001) Magnetism and magnetic materials; Cambridge University Press. https://doi.org/10.1017/CBO9780511845000
69. Medeiros Filho FC, Oliveira LL, Pedrosa SS, Rebouças GOG, Carriço AS, Dantas AL (2015) Impact of core-shell dipolar interaction on magnetic phases of spherical core-shell nanoparticles. Phys Rev B - Condens Matter Mater Phys 92(6):064422. https://doi.org/10.1103/PhysRevB.92.064422
70. Yafet Y, Kwo J, Gyorgy EM (1986) Dipole-dipole interactions and two-dimensional magnetism. Phys Rev B 33(9):6519–6522. https://doi.org/10.1103/PhysRevB.33.6519
71. Lavorato G, Winkler E, Ghirri A, Lima E, Peddis D, Troiani HE, Fiorani D, Agostinelli E, Rinaldi D, Zysler RD (2016) Exchange

bias and surface effects in bimagnetic CoO-Core/$Co_{0.5}Ni_{0.5}Fe_2O_4$-shell nanoparticles. Phys Rev B 94(5):054432. https://doi.org/10.1103/PhysRevB.94.054432

72. Sartori K, Cotin G, Bouillet C, Halté V, Bégin-Colin S, Choueikani F, Pichon BP (2019) Strong interfacial coupling through exchange interactions in soft/hard core–shell nanoparticles as a function of cationic distribution. Nanoscale 11(27):12946–12958. https://doi.org/10.1039/C9NR02323B